Electro-optic study of antiferroelectric freely suspended films of bent-core mesogens in the B_2 phase

Ralf Stannarius,[1] Christian Langer,[1] and Wolfgang Weissflog[2]
[1]*Institute of Experimental Physics I, University of Leipzig, Linnéstrasse 5, D-04103 Leipzig, Germany*
[2]*Institute of Physical Chemistry, University of Halle, Mühlpforte 1, D-06108 Halle, Germany*
(Received 26 February 2002; revised manuscript received 8 July 2002; published 24 September 2002)

We report the electro-optic investigation of a liquid crystalline free standing film formed by bent-core (*banana-shaped*) mesogens. The ground state of the B_2 phase in the films is chiral and antiferroelectric, although the mesogenic molecules themselves lack chirality. The films can be switched in lateral electric fields. In the antiferroelectric ground state, the external electric field in the film plane couples to a small residual spontaneous polarization which we attribute to the incomplete compensation of polarizations of neighboring smectic layers, due to a nonzero twist normal to the layers. We derive viscoelastic parameters from the uniform switching dynamics and the structure of domain walls. Dynamic patterns in rotating fields are observed and analyzed.

DOI: 10.1103/PhysRevE.66.031709 PACS number(s): 61.30.−v, 77.80.−e, 68.15.+e, 87.64.Rr

I. INTRODUCTION

Liquid crystalline phases of bent-core (so-called *banana shaped*) molecules have evoked considerable interest during recent years, in particular due to their exotic symmetry properties [1–5], and in general their still not completely revealed phase structures. Although the molecules themselves lack chirality, they can form chiral mesophases with spontaneous breaking of mirror symmetry. The B_2 phase is of particular interest since it is switchable in electric fields and electro-optic effects can be exploited to characterize phase structure and dynamics [6]. Recently, an electroclinic effect has been demonstrated in B_2 mesogens [7].

In sandwich cells, the preparation of uniform alignment is a nontrivial task (e.g., Refs. [8–10]), and the quantitative electro-optic characterization of the materials is difficult. A suitable alternative is the investigation of freely suspended films with their macroscopically well-ordered layer structure. Reorientation dynamics and electro-optic effects can be conveniently studied when such films are exposed to in-plane electric fields and observed in a polarizing reflection microscope [2,11]. Comparable experiments have been described in smectic films ([e.g., Refs. [12–18]). For ferroelectric smectic C^* films, the electro-optic switching characteristics has been discussed and dynamic equations for the reorientation in electric fields have been derived [17–21].

We report a study of free standing B_2 films in external electric fields. By means of a four electrode setup, the fields can be switched into arbitrary directions in the film plane. The subsequent relaxation of the sample orientation is recorded in a reflection microscope. The sample response to 180° flips of the electric field is measured and domain walls are analyzed under the influence of the external electric field. Of particular interest is also the film dynamics in rotating fields, where patterns of different topology can be created. A quantitative analysis yields viscoelastic material properties and provides information on the phase symmetry and the spontaneous polarization of the film. We discuss the similarities to smectic C^* films and some characteristic differences observed in the B_2 films.

II. SETUP AND SAMPLE PREPARATION

The mesogenic compound 4-chloro-1,3-phenylene bis [4-(4-tetradecylphenyliminomethyl) benzoate] has been synthesized as described in Ref. [10]. Its phase sequence is *isotropic*-127 °C-B_2-68° C-*crystalline*. The chemical structure is shown in Fig. 1. Freely suspended films are prepared near the clearing point by drawing a small amount of the mesogenic material across a 1 mm hole in a thin glass sheet with evaporated electrodes. A top view of the support chip is shown in Fig. 2. Driving voltages are applied to two pairs of opposite electrodes (U_x between northeast and southwest, and U_y between northwest and southeast), the remaining four electrodes are at floating potential. The voltages are generated by two phase locked synthesizers (HP 33120A). In order to check the phase relation between the components U_x and U_y, the voltages are monitored during the experiments with a HP 54601B oscilloscope.

The films are observed in polarized light with a reflection microscope (NU2 Forschungsmikroskop, *Carl-Zeiss Jena*). The polarizers are nearly diagonal to the active electrode pairs, they are slightly decrossed. Reflection images are recorded with a *Hamamatsu* black and white digital camera with analog controller C-2400, and stored digitally by means of a frame grabber (*Pinnacle* DC 30) at a frame rate of 25 s^{-1}. The digitized images are processed with commercial software (IDL).

The film thickness is determined interferometrically from the wavelength dependent film reflectivity [22] at 123 °C, using a grating monochromator (*Oriel*) connected with a photomultiplier. The accuracy of film thickness determina-

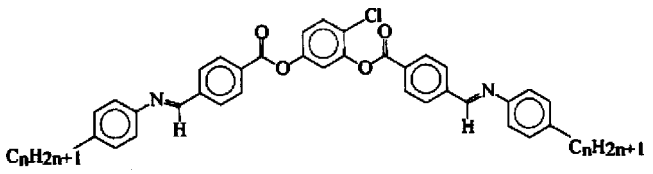

FIG. 1. Chemical structure of the investigated mesogen. The number of carbons in each alkyl chain is $n=14$.

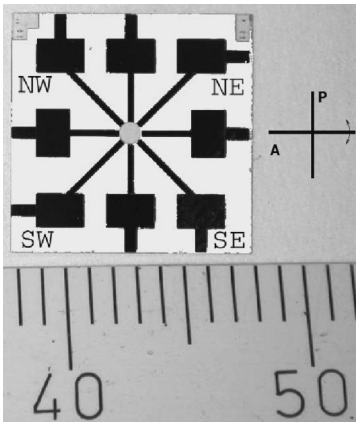

FIG. 2. Glass support with eight evaporated electrodes; we use only four active electrodes (labeled SW, NW, NE, and SE), the remaining four are not contacted. The hole for the free standing film is located in the center of the support. A ruler with millimeter scale gradations is shown in the bottom part for comparison.

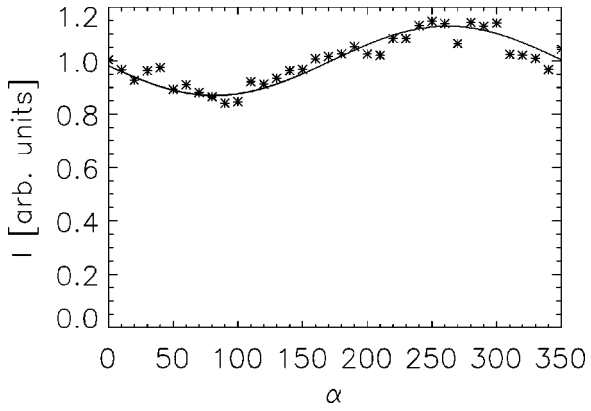

FIG. 3. Angular dependence of the reflectivity of the B_2 films. The angle α is measured between the in-plane electric field and the x direction. The polarizers are in NS and near WE orientations (as shown in Fig. 2).

tion is ± 3 nm. Since the refractive indices of the material are not known, we have assumed $n \approx 1.5$ in the interferometric measurements. All films studied here are thinner than 100 nm.

Temperature control is achieved with a home made controller with accuracy of ± 1 K. All experiments have been performed 4 K below the clearing point, at a temperature of 123 °C.

III. EXPERIMENTAL OBSERVATIONS AND INTERPRETATION

The thickness of the freshly drawn films is in general inhomogeneous, divided into two or more regions of uniform thickness, separated by sharp, discrete thickness steps. After a relaxation period of about 1 h, the films reach uniform thickness. In all experiments it was found that the thinnest region of the original film spreads until it finally extends to the complete film area. With crossed polarizers, the films appear nearly black. However, film textures can be observed when the polarizers are slightly decrossed. Best optical contrast has been achieved for all films with angles of about 80°–85° between polarizer and analyzer.

In the absence of electric fields, the freely suspended films are initially unoriented and show a faint Schlieren texture. When a low electric field (≈ 0.4 V/mm) is applied in the layer plane, the films reorient and reach an aligned state with uniform optical appearance. The reflection intensity in the aligned domains depends upon the orientation of the electric field with respect to the polarizers. Often, one or two domain walls persist and separate regions of equal optical appearance. Knowledge of the orientation of the optic axis in the films is essential for an interpretation of the electro-optic switching experiments. However, no previous information about the optical properties of the investigated material was available. In order to establish an empirical relation between reflectivity and orientation of the free standing film, we have rotated a dc electric field stepwise in the film plane (by varying the voltages U_x and U_y, simultaneously). Thereby we assume that the sample orientation follows the direction of the electric field. At each angle, we measure the brightness of the reflection images as a function of the electric field direction. Low electric fields (≈ 1 V/mm) are used to avoid electrically driven convective flow in the film plane [23,24]. The local film reflectivity is extracted from digitized images. It is measured in uniform regions far from domain walls and film boundaries. Figure 3 shows a typical reflectivity curve as a function of the field direction $\alpha = \arctan(U_y/U_x)$. The film thickness is ≈ 70 nm. The brightness variation $I(\alpha)$ can be fitted, in satisfactory approximation, to a function

$$I = I_0 + I_1 \cos(\alpha - \alpha_0), \tag{1}$$

with period 2π. The modulation of the intensity is very weak ($I_1 \ll I_0$) and hardly observable without analog video signal amplification. There is only one reflectivity maximum, it is near $\alpha_0 = 270°$ in the film shown in the figure. An explanation of the unexpected optical characteristics cannot be given straightforward. Since there are several optical elements in the optical path of the microscope between the polarizers that influence the polarization state (e.g., a prism to split incident and reflected beams) the incident light is slightly elliptically polarized. Moreover, the polarizers are imperfectly crossed to achieve satisfactory contrast, and the film birefringence itself is very small. Thus, we have not tried to analyze the complex optics in detail, but we evaluate the electro-optic experiments by means of the empirical dependence of Fig. 3. The same film which served for the construction of Fig. 3 was subsequently used in the electro-optic experiments presented below. All experimental observations can be interpreted on the basis of the assumption that the reflection intensity has roughly a sine dependence on the local sample orientation.

We find qualitatively the same reflectivity characteristics in all films, yet the position of the reflectivity maximum can differ between individual films. In a few films, we have found domains with different phase shifts of the reflection intensity curves (see the end of the experimental section).

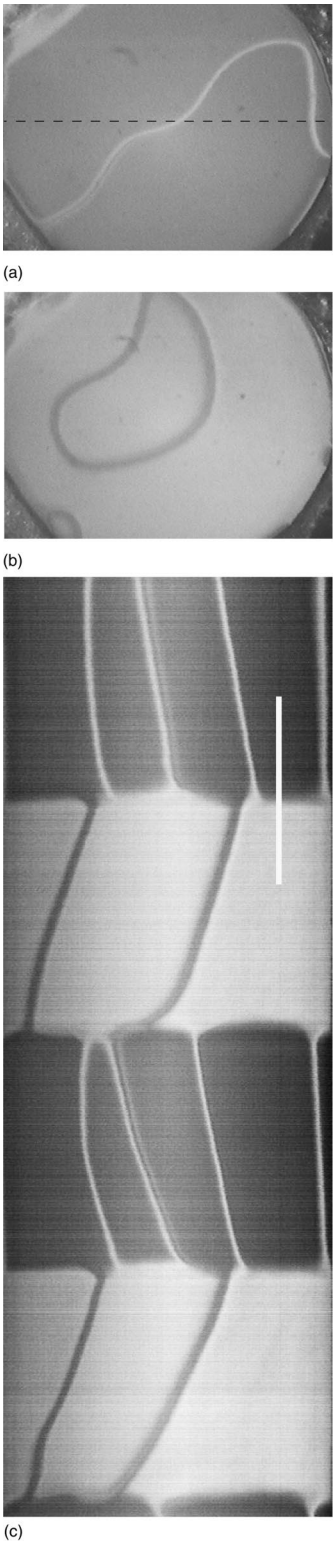

FIG. 4. (a) Reflection image of a 70-nm-thick B_2 film in an electric field $E_y = 3.12$ V/mm; the bright line is a 2π disclination wall between aligned domains. (b) Same film in the electric field $E_y = -3.12$ V/mm. (c) Space-time plot of a cross section (at the dashed line position) through the reflection images. The square voltage is reversed every 10 s; the vertical time axis (running from bottom to top) covers 40 s; the spatial range (horizontal axis) is 0.96 mm.

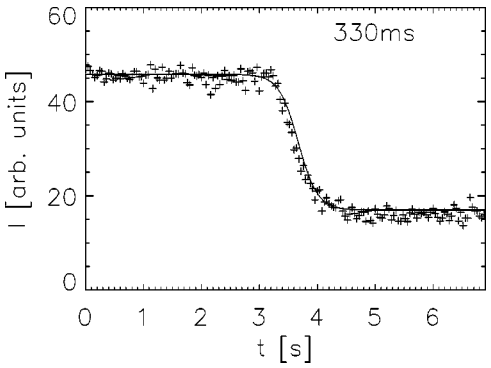

FIG. 5. Reflectivity change at electric field reversal from $U_y = -3.12$ V/mm to 3.12 V/mm, taken along the white bar in Fig. 4(c). The curve is fitted with a switching time $\tau = 0.33$ s.

When the electric field is reversed, the sample performs a 180° reorientation [30]. The reflection intensity changes from dark to bright when U_y is reversed and $U_x = 0$, or it switches between two states of comparable brightness with an intermediate bright or dark transient state when U_x is reversed and $U_y = 0$. This is unambiguous evidence of the polar switching of the B_2 films ($P \neq 0$).

Figures 4(a) and 4(b) show typical images of the film when the electric field is applied in y direction. When $E_y > 0$ [Fig. 4(a)], the aligned domains appear dark and a 2π wall separates these domains. Figure 4(b) shows the same film after electric field reversal, and Fig. 4(c) presents the space-time plot of a film cross section [along the dashed line in Fig. 4(a)] when a 0.1-Hz square wave is applied. The irregular bright and dark lines in the plot reflect intersections with domain walls that move in the film plane during the experiment. In regions sufficiently far from domain walls, it is possible to record the intensity change of the quasi uniformly reorienting sample. Figure 5 shows the reflectivity change at the transition from $U_y = -3.12$ V to $+3.12$ V (electric field strength (± 3.12 kV/m). The intensity has been averaged over a film spot of 3×3 image pixels ($\approx 65\ \mu m^2$). The location of this spot is marked by a white bar in the space-time plot of Fig. 4(c). The choice of the spot size and location is not critical as the selected film region is sufficiently homogeneous.

The dynamic equation describing the reorientation of a liquid crystalline film in absence of flow can be derived from the balance of electric, viscous, and elastic torques,

$$\gamma \dot{\varphi} = -PE \sin \varphi - \varepsilon_a \varepsilon_0 E^2 \sin \varphi \cos \varphi + K \nabla^2 \varphi, \qquad (2)$$

where γ is a rotational viscosity for reorientation in the film plane, P is an in-plane spontaneous polarization, φ is the angle between the polarization azimuth and the electric field direction, and $\varepsilon_a = \varepsilon_\parallel - \varepsilon_\perp$ is the dielectric anisotropy in the film plane, where $\varepsilon_\parallel$ is taken along the spontaneous polarization axis. K is a mean elastic constant for spatial variations of the sample orientation in the layer plane (one-constant approximation). After the substitutions $\tau^{-1} = PE/\gamma$, $\xi = \sqrt{K/(PE)}$, $D = \xi^2/\tau$, $\epsilon = \varepsilon_a \varepsilon_0 E/P$, this equation reads

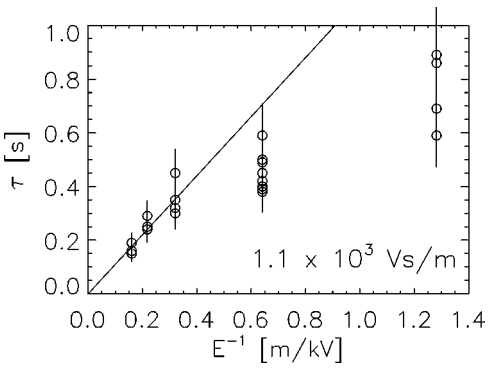

FIG. 6. Switching times determined from field reversal experiments as a function of the inverse electric field. The linear slope corresponds to $\tau E=\gamma/P=1.1\times10^{3}$ V s/m.

$$\dot{\varphi}=-\frac{1}{\tau}(\sin\varphi+\epsilon\sin\varphi\cos\varphi)+D\nabla^{2}\varphi. \tag{3}$$

Introduction of dimensionless time and space coordinates $t'=t/\tau$, $x'=x/\xi$, $y'=y/\xi$ leads to the material independent form $\dot{\varphi}=-(\sin\varphi+\epsilon\sin\varphi\cos\varphi)+\nabla^{2}\varphi$. In the following, we neglect the dielectric term and set $\epsilon=0$, since even a very small spontaneous polarization completely masks the induced polarizations (estimated to be of the order of 0.1 nC/cm^2 in electric fields of about 10^4 V/m). The uniform reorientation of the film ($\nabla^{2}\varphi=0$) can be described by an analytical solution of Eq. (3),

$$\tan\frac{\varphi}{2}=\tan\frac{\varphi_0}{2}\exp\left(-\frac{t}{\tau}\right). \tag{4}$$

When the in-plane electric field is reversed, the starting angle φ_0 is close to 180° immediately before the field is switched, and small fluctuations from the initial antiparallel alignment initiate the sample reorientation. The corresponding reflectivity change can be determined analytically when the sine dependence of Eq. (1) is substituted. The solid line in Fig. 5 shows the fit with Eq. (4) and the parameter $\tau=0.33$ s (at 3.12 kV/m).

A field dependence of the relaxation time τ at the temperature $T=123\,^{\circ}$C is shown in Fig. 6. It provides the ratio of viscous and electric torques. At electric fields above 1.5 kV/m, the switching times are proportional to the inverse electric field as expected, and the fit of the slope gives $E\tau=\gamma/P=(1.1\pm0.1)\times10^{3}$ V s/m. An upper limit for the electric field strength applicable in this experiment is around 10 kV/m. At higher fields, noticeable convection is induced in the film when the voltage is reversed. The switching times determined at low electric fields (<1 kV/m) deviate systematically from the linear fit curve. In these low field measurements, sample alignment is poor and domain walls become quite broad. It is not possible to select regions that are not affected by domain walls and film boundaries. The inhomogeneity of the director field leads to the observed faster reorientation.

In a constant electric field, closed loops of domain walls contract within a few minutes, while walls that connect opposite edges of the film are pinned, and they persist for long times, so that they are suitable to access the electric coherence length ξ. The width and profile of such walls are given by the balance of electric and elastic forces, which can be calculated from Eq. (3) by setting $\dot{\varphi}=0$. We consider a straight wall segment and choose the coordinate $\tilde{x}$ normal to the local direction of the wall,

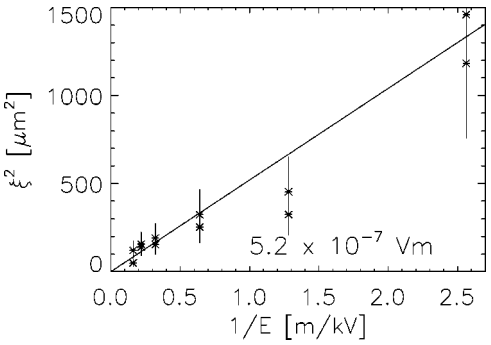

FIG. 7. Electric coherence length determined from the wall profiles as a function of the electric field. The linear slope of the ξ^2 vs $1/E$ curve gives the ratio $\xi^{2}E=K/P=5.2\times10^{-7}$ V m.

$$0=-\sin\varphi+\xi^{2}\frac{d^{2}\varphi}{d\tilde{x}^{2}}, \tag{5}$$

with the solution

$$\tan\frac{\varphi}{4}=\exp(\tilde{x}/\xi). \tag{6}$$

The angle φ changes from 0 to 2π across a width of $\approx4\xi$. As a consequence of the optical characteristics, the walls appear as bright stripes separating dark domains or dark stripes on bright domains, respectively, when the electric field is along y or $-y$ (Fig. 4), and they are composed of a darker and a brighter stripe between regions of intermediate brightness when the electric field is along x or $-x$. For a quantitative comparison with the experiment, we calculate intensity profiles on the basis of Eq. (6) and the empirical optical characteristics, Eq. (1), and fit the optical profiles to obtain the electric coherence length ξ as a function of an electric field (applied in y direction). Figure 7 shows the experimental ξ^2 vs inverse electric field. We consider only wall profiles in the vicinity of the film center where the electric field homogeneity in the four electrode geometry is optimal. The linear fit curve with slope $\xi^{2}E=(5.2\pm0.3)\times10^{7}$ V m provides the ratio of mean elastic constant and spontaneous polarization K/P. Segments in different orientations with respect to the electric field do not show systematic variations of wall profiles and widths. Such differences, if observed, could be exploited to determine bend and splay elastic contributions separately. Within experimental uncertainty, the measured data yield only the mean elastic modulus.

The ratio of elastic and viscous torques in the field-free sample can be determined in an independent experiment. For

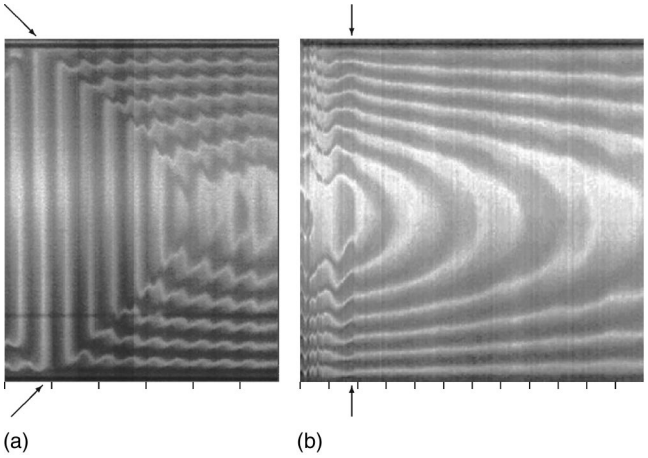

FIG. 8. (a) Formation of an array of traveling walls during the application of a rotating electric field of 3.6 kV/m with $\omega = 1.257\ s^{-1}$ (rotation period 5 s). The spatial range (vertical axis) is 0.96 mm; the time axis covers a range of 58 s. The ticks mark 10-s intervals. (b) Relaxation of the wall array after the electric field is switched off (at arrow position); axes as in (a); the time range is 120 s.

that purpose, the sample orientation in the circular film is continuously twisted to a regular target pattern.

The films are exposed to rotating electric fields such that the sample orientation in the film middle initially follows the electric field. The reorientation is either synchronous at high electric fields and slow angular velocities ω of the field, or asynchronous at low electric fields and fast ω. The dynamic behavior is similar in many respects to the reorientation of nematics in homeotropic sandwich cells exposed to rotating magnetic fields [25,26], and ferroelectric smectics in free standing film geometry [12–14,17,18]. The asymptotic phase lag between electric field and sample orientation in the synchronous regime increases with ω and reaches a maximum angle $\pi/2$ at the critical frequency for the transition into the asynchronous reorientation regime, $\omega_c(E) = 1/\tau(E)$. In the free standing films, the role of lateral boundaries quickly prevails. At the film peripheral support, the sample orientation is retarded or completely suppressed, and with every revolution of the orientation in the center, the phase difference between film middle and outer perimeter increases. When the sample orientation is fixed at the film perimeter (rigid anchoring), domain walls are created with spatial periodicity $\Xi = (\pi^2/2)\xi$ and move towards the film center with a velocity [18]

$$v = (\pi/4)\omega\xi. \tag{7}$$

As soon as the array of walls reaches the center of the film, synchronous or asynchronous reorientation regimes are completely abandoned and the phase in the film middle (respective to the outer boundary) oscillates around a fixed value determined by E, ω, and K.

Figure 8 visualize the evolution of a target pattern in the film during and after exposure to a 3.6 kV/m electric field with rotation period 5 s ($\omega = 1.257\ s^{-1}$). They show the time dependence of the reflectivity profile along a central cross section of the film images. The horizontal axes in both plots represent the time coordinate. Figure 8(a) shows the production of disclination walls. In the beginning of the experiment, the film has two circular walls remaining from a previous experiment where the electric field has been rotated counterclockwise. At time $t = 0$ (left edge of the image), a clockwise rotation of the electric field has been started. First, the residual walls are unwound. After two rotations of the field, new walls are generated at the outer boundaries where the orientation of the material is strongly anchored. With every revolution of the field, one new wall is created. In the film middle, the periodic intensity modulation is initially synchronous with the electric field, with one intensity maximum per revolution. The first four walls that appear from the boundaries in this experiment are equidistant. The wall velocity can be extracted directly from the position of the leading edge of the wall array in the space-time plot (arrows). We find, for example, the radial velocities $(11.5 \pm 1)\ \mu$m/s and $(12.5 \pm 1)\ \mu$m/s at the opposite sides of the cross section shown in Fig. 8(a). The average value from a number of independent experiments is 12 μm/s. Inserted in Eq. (7), it yields a coherence length $\xi = 12.1\ \mu$m at 3.12 kV/m, and the product $\xi^2 E = 5.3 \times 10^{-7}$ V m is in satisfactory agreement with the slope $\xi^2 E$ determined in Fig. 7 for stationary walls.

After approximately six field cycles in Fig. 8(a), the leading wall approaches the center of the film and the film asymptotically reaches a limit cycle, with seven oscillating circular walls in the target pattern. Figure 8(b) shows the elastic relaxation of the same film when the electric field is switched off (at arrows position). In the moment the field is removed, the wall array relaxes very quickly to a smooth radial $\varphi(r)$ profile with its maximum in the film middle. The relaxation of φ is described by the dynamic equation $\dot{\varphi} = +D\nabla^2\varphi$ derived from Eq. (3). In the cylindrical film geometry, the analytical solution is a superposition of Bessel functions [18], and the long-term relaxation is described by the ground mode

$$\varphi(r,t) = \varphi_m J_0\left(\rho_0 \frac{r}{r_0}\right) e^{-t/\tau_0}, \tag{8}$$

where r is the radial coordinate, r_0 is the film radius, ρ_0 is the first zero of the Bessel function J_0, and $\tau_0 = D^{-1}(R/\rho_0)^2$. A fit of the relaxation of $\varphi(r,t)$ in absence of an electric field yields $\tau_0 = 100$ s and $D = K/\gamma = (4.3 \pm 0.5) \times 10^{-10}\ m^2\ s^{-1}$.

So far, the experiments have dealt with films that show a uniform optical characteristics $I(\varphi)$. In some cases, however, films have been observed which do not show a unique $I(\varphi)$ dependence in all regions in the film plane. An example is shown in Fig. 9(a). The snapshot has been taken during the application of a rotating electric field (≈ 8 kV/m, $\omega = 6.28\ s^{-1}$). The image in Fig. 9(a) shows a nearly circular thin (less than five layers) region with a diameter of about 0.5 mm, in an otherwise thicker film. Exposure times of the camera have been chosen such that we focus on the structures in the thin film region, the rest of the film, approximately 20 layers thick, is overexposed, it is not relevant here. Inside the thin region, one observes coexisting spiral and

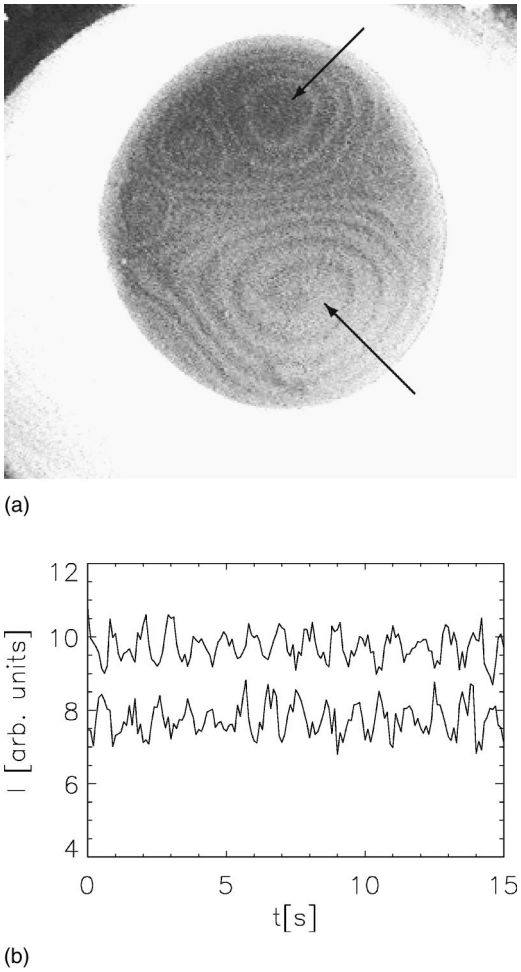

FIG. 9. (a) Reflection image of a film in a rotating electric field (8 kV/m, 1 Hz). The central region with about 0.5 mm diameter is very thin; it has probably two or four molecular layers (the outer, thicker film area is overexposed). The central area is divided in two domains. In both, the reflection intensities alternate periodically, synchronous to the electric field, but with a mutual phase shift of π. The film thickness in both domains is the same. The target pattern in the upper domain and the spiral in the lower domain are well separated. (b) Periodic variation of the reflectivity in the two domains of the film shown in (a) at the arrow positions. The reflectivity changes in the upper and lower domain are phase shifted by a half cycle.

target patterns. (The rest of the film contains more spirals and targets.) The coexistence of multiple dynamic patterns is not unusual [17]. A spiral is formed from target patterns when a defect moves into the core of the structure. Such patterns are well known in ferroelectric smectic films exposed to rotating electric fields (see, e.g., Ref. [13]).

The one armed spiral in the bottom part of the film in Fig. 9(a) is formed by a 2π wall twisted around core defect with strength $s=-1$, within a domain that is otherwise uniformly aligned to the electric field. The target pattern is defect-free and consists of an array of ring walls, again embedded in an aligned domain. However, one notices in Fig. 9(a) that the region aligned to the electric field direction appears dark in the upper domain whereas it is bright in the lower one. In contrast, the thin 2π walls are bright in the upper structure and dark in the lower. After a half period of the electric field cycle, the contrast is reversed in both regions. The angular velocity ω is chosen well below $\omega_c(E)$. If one naturally assumes that in both regions the spontaneous polarization outside the walls is aligned to the electric field, the optical characteristic must be different for the same direction of $\vec{P}$. When the rotation of the field is stopped, one can choose a stationary electric field such that either the upper or lower domain is in the bright state, depending upon the field direction.

The time dependence of the optical reflectivity in the rotating field can be extracted in the same way as in Fig. 5. We choose two positions within the uniform domains, marked by arrows in Fig. 9(a), and compose the corresponding reflectivity curves to Fig. 9(b). An offset has been added to the upper curve for better visibility. Apart from a few disturbances in the lower curve, when the arm of the spiral crosses the probe spot, both curves are periodically modulated as expected with the field rotation, but the modulations have a mutual phase shift of 180°. Such an appearance of domains with different optical characteristics has been observed in a couple of films. In all these cases, one of the domains disappeared in the course of a few hours during the experiments. In contrast, we have not observed the spontaneous formation of two domains with optically different characteristics from a previously uniform film.

IV. CONCLUSIONS AND SUMMARY

The most astonishing result of the experiment seems to be the applicability of Eq. (3) with the ferroelectric term. In sandwich cells, the investigated material is known to form synclinic (racemic) or anticlinic (chiral) states which are both antiferroelectric. The nature of the observed spontaneous polarization will be discussed in this section. Moreover, all experiments presented in the preceding section provide only ratios of material parameters, additional information is necessary for an interpretation of the measured data.

A saturation polarization $P_S=500$ nC/cm^2 of the material has been determined from the current peaks during electric field reversal in sandwich cells [10]. A somewhat smaller value of 408 nC/cm^2 has been reported for the same material by Barnik and co-workers [27]. In chemically similar antiferroelectric compounds, electric current measurements gave saturation polarizations of about 640 nC/cm^2 [6]. It is obvious that in order to obtain realistic values for the elastic constant and rotational viscosity, the polarization P that enters Eq. (3) must be more than two orders of magnitude smaller. We can exclude that a ferroelectric state with nonzero polarization is induced by the applied electric field. A number of experimental observations contradict such an assumption. First, the behavior of the sample at field reversal would be different and could not be described with Eq. (3) that presupposes a reorientation of the spontaneous polarization azimuth in the film plane. Furthermore, the shape of 2π domain walls agrees well with the model of a continuous rotation of the orientation axis (and $\vec{P}$) in the film plane. Finally, a small induced polarization would in first approxi-

TABLE I. Material parameters measured in the electro-optical experiments with the free standing B_2 films of 4-chloro-1,3-phenylene-bis [4-(4-tetradecylphenyliminomethyl)benzoate].

Experiment	Parameter ratio	Experimental value
180° switching	γ/P	1.1×10^{3} V s/m
Target pattern relaxation	K/γ	4.3×10^{-10} m^2/s
Stationary wall width	K/P	5.2×10^{-7} Vm
Wall velocity in rotational field	K/P	5.3×10^{-7} Vm

mation be linear with the electric field, and the electric field dependence of the wall widths as well as switching times would be qualitatively different. We do also exclude that the spontaneous polarization is generated by the uncompensated surface layer of an odd-numbered layer film which is coincidently P_S/P layers thick, since we find comparable switching times for films of different thickness (otherwise, the effective polarization would scale linearly with the inverse film thickness). Furthermore, all films investigated in this study had thicknesses well below 40 molecular layers.

In order to determine the absolute value of the spontaneous polarization in the film, we refer to the value for the rotational viscosity $\gamma=0.02$ Pa s, given by Barnik *et al.* [27]. If we enter this value in the first two ratios given in Table I, we find the two remaining constants (with an accuracy of $\pm10\%$)

$$P=1.8\ \text{nC/cm}^2, \quad K=8.6\ \text{pN},$$

and the ratios K/P given in the table, which have been determined by independent methods, are consistent with these values within the limits of experimental error. The value obtained for the elastic constant K seems to be in a reasonable order of magnitude, comparable values in other B_2 mesogens have not been available so far. All results of the electro-optic experiments in this work, including the localized structures studied in Ref. [11] can be consistently described with the parameters given above.

The origin of the existing spontaneous polarization can be explained if one assumes that in the antiferroelectric state, dipole moments of mesogens in neighboring layers compensate longitudinally, but due to a small helicity of the sample, a transverse polarization component remains. A similar explanation has been proposed for antiferroelectric smectic phases [28].

If one assumes a helical pitch length corresponding to about 1400 molecular layers, then the angle between two adjacent layers is about $\delta=1/4°$. In that case, the vestige polarization $P=2\sin(\delta/2)P_S$ of the saturation value P_S (obtained when the sample is switched into the ferroelectric state) remains uncompensated. This value is sufficient to account for the effects described in this paper. Since the film thickness is much lower than the helical pitch assumed in this model, the twist can be neglected as far as the *direction* of the uncompensated netto polarizations in different layers of the film is regarded. We note, however, that although helicity has been discussed in the context of B_2 phases elsewhere [29], we have no direct evidence of the existence of a helical pitch in the investigated material.

We conclude that the sample studied here is in an antiferroelectric ground state, that it possesses a small residual spontaneous polarization, and that at least some films show the spontaneous appearance of two types of domains which differ in their optical characteristics when the spontaneous polarization is aligned to an external in-plane electric field. The most natural interpretation of these structures is the assumption of coexisting domains of opposite handedness. In all experiments, one of the enantiotropic domains disappears gradually and finally leaves a film with optically uniform characteristics.

ACKNOWLEDGMENTS

The authors acknowledge financial support by the Deutsche Forschungsgemeinschaft within Grant No. SFB 294.

[1] T. Niori, F. Sekine, J. Watanabe, T. Furukawa, and H. Takezoe, J. Mater. Chem. **6**, 1231 (1996); T. Sekine, Y. Takanashi, J. Watanabe, and H. Takazoe, Jpn. J. Appl. Phys., Part 2 **36**, L1201 (1997).

[2] D.R. Link, G. Natale, R. Shao, J.E. Maclennan, N.A. Clark, E. Körblova, and D.M. Walba Science **278**, 1924 (1997).

[3] D.M. Walba, E. Körblova, R. Shao, J.E. Maclennan, D.R. Link, M.A. Glaser, and N.A. Clark Science **288**, 2181 (2000).

[4] G. Pelzl, S. Diele, and W. Weissflog Adv. Mater. **11**, 707 (1999).

[5] A. Jakli, D. Kruerke, H. Sawade, and G. Heppke, Phys. Rev. Lett. **86**, 5715 (2001).

[6] G. Pelzl, S. Diele, S. Grande, A. Jakli, Ch. Lischka, H. Kresse, H. Schmalfuss, I. Wirth, and W. Weissflog, Liq. Cryst. **26**, 401 (1999).

[7] A. Jakli, G.G. Nair, C.K. Lee, and L.C. Chien, Liq. Cryst. **28**, 489 (2001).

[8] A. Jakli, S. Rauch, D. Lötzsch, and G. Heppke, Phys. Rev. E **57**, 6737 (1998).

[9] W. Weissflog, Ch. Lischka, I. Benné, T. Scharf, G. Pelzl, S. Diele, and H. Kruth, Proc. SPIE **3319**, 14 (1997).

[10] W. Weissflog, Ch. Lischka, S. Diele, G. Pelzl, and I. Wirth, Mol. Cryst. Liq. Cryst. Sci. Technol., Sect. A **328**, 101 (1999).

[11] R. Stannarius, C. Langer, and W. Weissflog, Ferroelectrics (to be published).

[12] C. Dascalu, G. Hauck, H.D. Koswig, and U. Labes, Liq. Cryst. **21**, 733 (1996).

[13] P.E. Cladis, P.L. Finn, and H.R. Brand, Phys. Rev. Lett. **75**, 1518 (1995); P.E. Cladis and H.R. Brand, Liq. Cryst. **14**, 1327 (1993).
[14] S. Uto, H. Ohtsuki, M. Terayama, M. Ozaki, and K. Yoshino, Jpn. J. Appl. Phys., Part 2 **35**, L158 (1996).
[15] C. Langer and R. Stannarius, Ferroelectrics **244**, 347 (2000); R. Stannarius and C. Langer, Mol. Cryst. Liq. Cryst. Sci. Technol., Sect. A **358**, 109 (2001).
[16] C. Chevallard, J.-M. Gilli, T. Frisch, I.V. Chikina, and P. Pieranski, Mol. Cryst. Liq. Cryst. Sci. Technol., Sect. A **328**, 595 (1999).
[17] G. Hauck, H.D. Koswig, and C. Selbmann, Liq. Cryst. **21**, 847 (1996); G. Hauck and H.D. Koswig, Ferroelectrics **122**, 253 (1995).
[18] D. Link *et al.*, Phys. Rev. Lett. **84**, 5772 (2000), and references therein.
[19] A. Kilian, H.D. Koswig, and A. Sonnet, Mol. Cryst. Liq. Cryst. Sci. Technol., Sect. A **265**, 321 (1995).
[20] C. Escher, T. Geelhaar, and E. Böhm, Liq. Cryst. **3**, 469 (1988).
[21] R. Stannarius, N. Klöpper, Th. Fischer, and F. Kremer, Phys. Rev. E **58**, 6884 (1998).
[22] I. Kraus, P. Pieranski, E. Demikhov, H. Stegemeyer, and J. Goodby, Phys. Rev. E **48**, 1916 (1993).
[23] S.W. Morris, J.R. de Bruyn, and A.D. May, Phys. Rev. Lett. **65**, 2378 (1990); Phys. Rev. A **44**, 8146 (1991).
[24] A. Becker, H. Stegemeyer, R. Stannarius, and St. Ried, Europhys. Lett. **39**, 257 (1997); C. Langer and R. Stannarius, Phys. Rev. E **58**, 650 (1998).
[25] F. Brochard J. Phys. (France) Lett. **35**, L19 (1974); F. Brochard, L. Leger, and R.B. Meyer, J. Phys. Colloq. **36**, C1-209 (1974).
[26] K.B. Migler and R.B. Meyer, Phys. Rev. Lett. **66**, 1485 (1991); Physica D **71**, 412 (1994).
[27] M.I. Barnik, L.M. Blinov, N.M. Shtykov, S.P. Palto, G. Pelzl, and W. Weissflog, Liq. Cryst. (to be published).
[28] Yu.P. Panarin, O. Kalinovskaya, and J.K. Vij, Liq. Cryst. **25**, 241 (1998); Appl. Phys. Lett. **72**, 1667 (1998).
[29] W. Weissflog, H. Nádasi, U. Dunemann, G. Pelzl, S. Diele, A. Eremin, and H. Kresse, J. Mater. Chem. **11**, 2748 (2001).
[30] By the term *sample orientation* we refer to the azimuth of the spontaneous polarization $\vec{P}$ in the film plane.